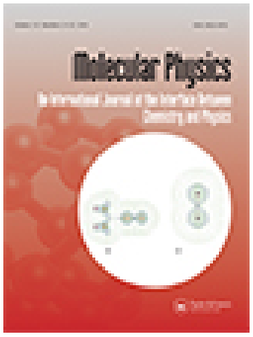

Taylor & Francis
Taylor & Francis Group

Molecular Physics

An International Journal at the Interface Between Chemistry and Physics

ISSN: 0026-8976 (Print) 1362-3028 (Online) Journal homepage: http://www.tandfonline.com/loi/tmph20

Theoretical studies of three-dimensional potential energy surfaces using neural networks and rotational spectra of the Ar–N_2 complex

Hong Fu, Rui Zheng & Limin Zheng

To cite this article: Hong Fu, Rui Zheng & Limin Zheng (2015): Theoretical studies of three-dimensional potential energy surfaces using neural networks and rotational spectra of the Ar–N_2 complex, Molecular Physics, DOI: 10.1080/00268976.2015.1085603

To link to this article: http://dx.doi.org/10.1080/00268976.2015.1085603

MOLECULAR PHYSICS, 2015
http://dx.doi.org/10.1080/00268976.2015.1085603

Taylor & Francis
Taylor & Francis Group

RESEARCH ARTICLE

Theoretical studies of three-dimensional potential energy surfaces using neural networks and rotational spectra of the Ar–N_2 complex

Hong Fu[a], Rui Zheng[b,c] and Limin Zheng[c]

[a]Department of Physical & Electrical Engineering, Ningde Normal University, Ningde 352100, People's Republic of China; [b]School of Mathematics & Information Science, North China University of Water Resources and Electric Power, Zhengzhou 450011, People's Republic of China; [c]Key Laboratory of Magnetic Resonance in Biological Systems, State Key Laboratory of Magnetic Resonance and Atomic and Molecular Physics, Wuhan Centre for Magnetic Resonance, Wuhan Institute of Physics and Mathematics, Chinese Academy of Sciences, Wuhan 430071, People's Republic of China

ABSTRACT

A new three-dimensional potential energy surface (PES) of the Ar–N_2 van der Waals complex is constructed using the neural network method based on *ab initio* data points at the CCSD(T) level. The aug-cc-pVQZ basis set is employed for all atoms with midbond functions. The vibrationally averaged PES V_{00} is characterised by a global T-shaped minimum which occurs at $R = 3.715$ Å, $\theta = 90.0°$ with a well depth of 98.779 cm^{-1}. Based on our three-dimensional PES, bound-state calculations are performed for three isotopomers of Ar–$^{14}N_2$, Ar–$^{15}N_2$, and Ar–$^{14}N^{15}N$, and several intermolecular vibrational states are assigned by analysing the wavefunctions. Moreover, the averaged structural parameters are calculated and the pure rotational transition frequencies with $J = 0$–6 are predicted. The spectroscopic constants are determined by fitting the rotational energy levels. The theoretical results are in good agreement with experimental data and this work gives more accurate results than those determined previously for the Ar–N_2 complex.

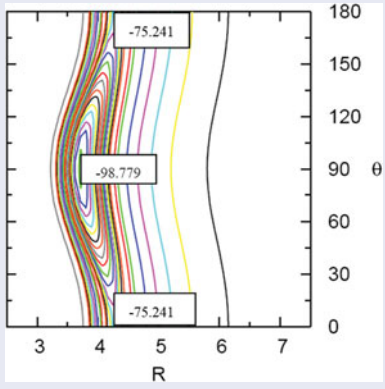

ARTICLE HISTORY
Received 25 May 2015
Accepted 17 August 2015

KEYWORDS
Ar–N_2; potential energy surface; neural networks; bound-state calculations; spectroscopic parameters

1. Introduction

The van der Waals complex is an ideal model in the research of intermolecular interactions, especially for the simple system consisting of a rare gas atom and a molecule. Over the last decades, Ar–N_2 has been extensively investigated both experimentally [1–4] and theoretically [5–11].

For the Ar–N_2 complex, in experiment, in 1974, Henderson and Ewing [1] first observed an infrared spectrum and confirmed that the stable structure is a T-shaped configuration. In 1988, McKellar [2] remeasured the infrared absorption spectrum at a higher resolution. In 1992, Jäger and Gerry [3] investigated the microwave spectrum using an MWFT spectrometer. In 1994, Jäger

CONTACT Hong Fu fuhongwipm@126.com

et al. [4] went further to investigate pure rotational spectra of three isotopomers of the Ar–N_2 complex in the frequency range of 3.5–24 GHz and obtained transition frequencies and spectroscopic constants. In theory, in 1993, Slanina et al. [5] computed harmonic vibration using an MP2/MP4 perturbation treatment with 6–31G*. In 1997, a two-dimensional PES was determined at the CCSD(T) level with the basis sets aug-cc-pVTZ and aug-cc-pVQZ by Naumkin [6], confirming the single well as a T-shaped configuration. In 1999, Fernández et al. [7] evaluated two PESs using CCSD(T) and the aug-cc-pVTZ basis set extended with midbond functions. In 2003, Patel et al. [8] calculated intermolecular potentials for Rg–N_2 (Rg = He, Ne, and Ar) at the level of CCSD(T) with the basis sets of aug-cc-pVTZ and aug-cc-pVDZ and obtained complete basis set limit surfaces using the Truhlar extrapolation formula. In 2004, Munteanu et al. [9] evaluated several ground-state PESs at CCSD(T); they used the aug-cc-pVXZ (X = 5, Q, T, D) and the daug-cc-pVQZ basis sets augmented with a set of 3*s*3*p*2*d*1*f*1*g* and 3*s*3*p*2*d*2*f*1*g* midbond functions, respectively. The results of the aug-cc-pVQZ-33211 basis set were close to those of the aug-cc-pV5Z-33211 basis set. In 2005, Zhu et al. [10] studied the intermolecular interaction potentials using CCSD(T) with perturbative triples correction. In 2006, Dham et al. [11] developed a PES which was based on the exchange-Coulomb potential energy model and was a combination of damped dispersion energy series and *ab initio* calculations of the Heitler–London interaction energy with adjustable parameters available for fitting to experimental data.

For the Rg–N_2 (Rg = He, Ne, Kr, and Xe) complexes, a lot of research has been done in experiment [12–14] and theory [8,15–18], confirming the stable structure of each complex is a T-shaped configuration.

In all the above PESs, the N_2 monomer was treated as a rigid rotor and the bound-state calculated results are close to the experimental values. However, the three-dimensional PES containing intramolecular vibrations of the N_2 monomer is more accurate. For example, in 2011, Zhang et al. [19] developed a three-dimensional PES of the Kr–N_2 complex using the CCSD(T) method and mixed basis sets with mid-bond functions; they constructed five two-dimensional PESs at five values of N_2 bond length by fitting *ab initio* potential points to an analytic function, and then used the five two-dimensional PESs to construct the three-dimensional PES by interpolating. Compared with two-dimensional PESs of the Kr–N_2 complex [18], the bound-state calculation confirmed that a more accurate result could be obtained based on three-dimensional PESs. Until now there is no report on the three-dimensional PES for the Ar–N_2 complex. Behler [20] reported a review to point out that the PESs constructed using neural network (NN) methods were numerically very accurate and can be applied to different types of systems. In the present paper, we report a three-dimensional PES constructed using the NN method based on *ab initio* data points at the CCSD(T) level and bound-state calculations. Also, this new three-dimensional PES containing intramolecular vibrations of the N_2 monomer is very useful for the calculation of the infrared spectra of the Ar–N_2 complex.

2. Computational details

2.1 Ab initio calculations of intermolecular potential energy

The three-dimensional potential energy surface of the Ar–N_2 complex can be described by three Jacobi coordinates (R, θ, r), where R is the distance between the rare gas atom and the centre of mass of N_2, θ denotes the enclosed angle between the vector R and the molecular axis of N_2, and r is the N_2 bond length.

The *ab initio* potential energy grids for the Ar–N_2 complex is chosen as follows. The radial grids include 18 points with the R coordinates {5.0, 5.5, 6.0, 6.5, 6.8, 7.0, 7.2, 7.5, 8.0, 8.5, 9.0, 9.5, 10.0, 11.0, 13.0, 15.0, 17.0, 22.0}a_0, the N_2 bond length has five coordinates {1.85, 1.95, 2.074315, 2.15, 2.25}a_0, and θ varies from 0° to 180° in steps of 10°.

The potential energy for each geometry is calculated using the supermolecular method at the level of the single- and double-excitation coupled-cluster method with a noniterative perturbation treatment of triple excitations [CCSD(T)] [21]. The augmented correlation-consistent polarised valence quadruple-zeta (aug-cc-pVQZ) basis set of Dunning is employed for all atoms. The bond functions (3*s*3*p*2*d*2*f*1*g*) (for 3*s* and 3*p*, $\alpha = 0.94$, 0.34, 0.12; for 2*d* and 2*f*, $\alpha = 0.64$, 0.23; for 1*g*, $\alpha = 0.35$) [22] are also used at the middle point of the intermolecular distance R. The full counterpoise procedure of Boys and Bernardi [23] is employed to correct the basis set superposition error (BSSE). All the calculations are carried out using the Molpro 2010 software package [24].

2.2 Construction of the three-dimensional potential energy surface

Recently, a permutation invariant polynomial NN approach to fitting the PES was proposed and successfully applied to the H + H_2, Cl + H_2, X + H_2O (X = H, O, and F), and OH+CO reaction systems by Jiang and Guo [25–27]. Chen and Zhang [28–31] constructed global PESs of chemical reaction systems such as H_2 + OH, OH + CO, H + CH_4, confirming the NN fitting

method is a powerful method to construct accurate PESs for polyatomic reactions. Now, the NN fitting method based on high-level *ab initio* calculation is used to construct the three-dimensional PES of the Ar–N_2 van der Waals complex.

The architecture of a feed-forward NN could be denoted by *I*–*J*–*K*–1, where *I* is the number of nodes in the input layer, *J* and *K* are the numbers of neurons in the two hidden layers, and 1 is the number of neurons in the output layer. The value in the output layer, which is equal to the potential energy for input geometry, could be calculated in the following way [28–30].

The output of the *j*th neuron in the first hidden layer is

$$y_j^1 = f^1\left[b_j^1 + \sum_{i=1}^{I}(w_{j,i}^1 x_i)\right], \quad j = 1, 2, ..., J. \tag{1}$$

The output of the *k*th neuron in the second hidden layer is

$$y_k^2 = f^2\left[b_k^2 + \sum_{j=1}^{J}(w_{k,j}^2 y_j^1)\right], \quad k = 1, 2, ..., K. \tag{2}$$

The output in the output layer is

$$y = b_1^3 + \sum_{k=1}^{K}\left(w_{1,k}^2 y_k^2\right), \tag{3}$$

where $w_{j,i}^l$ denotes the weight connecting the *i*th neuron of the $(l-1)$th layer and the *j*th neuron of the *l*th layer, b_j^l denotes the bias weight, where *l* indicates the layer of the target neuron and *j* its number, and f^1 and f^2 are transfer functions taken as hyperbolic tangent functions. From Ref. [20], $x_i (i = 1, 2, 3)$ could be a function of Jacobi coordinates (R, θ, r) of the Ar–N_2 van der Waals complex, the full symmetry being included in the NN,

$$x_1 = \left|\sqrt{R^2 + \left(\frac{m_1 r}{m_1+m_2}\right)^2 - \frac{2m_1 Rr\cos\theta}{m_1+m_2}} + \sqrt{R^2 + \left(\frac{m_2 r}{m_1+m_2}\right)^2 + \frac{2m_2 Rr\cos\theta}{m_1+m_2}}\right|, \tag{4}$$

$$x_2 = \left|\sqrt{R^2 + \left(\frac{m_1 r}{m_1+m_2}\right)^2 - \frac{2m_1 Rr\cos\theta}{m_1+m_2}} - \sqrt{R^2 + \left(\frac{m_2 r}{m_1+m_2}\right)^2 + \frac{2m_2 Rr\cos\theta}{m_1+m_2}}\right|, \tag{5}$$

$$x_3 = r, \tag{6}$$

for Ar–$^{14}N_2$, where m_1 and m_2 are the nuclear masses of ^{14}N. For Ar–$^{15}N_2$, m_1 and m_2 are the nuclear masses of ^{15}N. For Ar–$^{14}N^{15}N$, m_1 is the nuclear mass of ^{14}N and m_2 is the nuclear mass of ^{15}N.

The root mean squared error (RMSE) can be calculated to monitor the fitting accuracy:

$$\mathrm{RMSE} = \sqrt{\frac{1}{N_{\mathrm{data}}}\sum_{i=1}^{N_{\mathrm{data}}}(E_{\mathrm{fit}} - E_{\mathrm{ab\ initio}})^2} \tag{7}$$

where N_{data} is the number of *ab initio* potential energy grids, which are divided into training sets (95%) and validation sets (5%), NN is trained using the Levenberg–Marquardt algorithm [32] to reduce the RMSE value, and the 'early-stopping' method [33] is used to stop overfitting. We achieve the PES $V(R, \theta, r)$ of RMSE of 0.044 cm^{-1} using Chen's code [28–30] with the NN structure of 3–15–15–1.

2.3 Vibrationally averaged two-dimensional potential energy surface

From some reports [19,34–38], we know that the calculated results from the vibrationally adiabatic potential are in good agreement with the experimental results; the vibrationally averaged Ar–N_2 potential is expressed as follows [39]:

$$V_{v'v}(R, \theta) = \langle \chi_{v'}(r) | V(R, \theta, r) | \chi_v(r) \rangle, \tag{8}$$

where $\chi_v(r)$ is the vibrational wavefunction of N_2, which satisfies the following equation:

$$\left[-\frac{1}{\mu_{N_2}}\frac{\partial^2}{\partial r^2} + V_{N_2}(r)\right]\chi_v(r) = E_{N_2}\chi_v(r), \tag{9}$$

where μ_{N_2} is the reduced mass of N_2 and $V_{N_2}(r)$ is the potential energy curve of N_2. This curve is constructed by executing one-dimensional interpolation with the Lagrange polynomial formula which has been employed in the previous works [40,41]. The potential energy for each *ab initio* point is calculated using the aug-cc-pVQZ basis set at the CCSD(T) level.

2.4 Bound-state calculations

Within the vibrationally adiabatic approximation, the Hamiltonian of the Ar–N_2complex in Jacobi coordinates can be written as

$$\hat{H}_v = -\frac{1}{2\mu}\frac{\partial^2}{\partial R^2} + \frac{1}{2\mu R^2}\left(\hat{J} - \hat{j}\right)^2 + B_v\hat{j}^2 + V_{vv}(R, \theta), \tag{10}$$

where μ is the reduced mass of the Ar–N_2 complex, $\hat{J}$ is the total angular momentum, $\hat{j}$ is the angular momentum for the N_2 monomer, and B_v is the rotational constant of N_2 with $B_0(^{14}N_2) = 1.989574\ \mathrm{cm}^{-1}$, $B_0(^{15}N_2) = 1.857624\ \mathrm{cm}^{-1}$, and $B_0(^{14}N^{15}N) = 1.923596\ \mathrm{cm}^{-1}$, as reported by Bendtsen [42].

The wavefunction of the system can be expanded as a linear combination of products of the radial and angular basis functions and can be written as

$$\Psi(R,\theta) = \sum_i \sum_{j,K} c^i_{j,K} \varphi_i(R)\, Y^{JM\varepsilon}_{jK}, \tag{11}$$

where $\varphi_i(R)$ is the radial basis function to describe the intermolecular stretch and obtained by solving a one-dimensional reference Hamiltonian defined as follows:

$$\hat{h} = -\frac{1}{2\mu}\frac{\partial^2}{\partial R^2} + V_{vv}\left(R, 90^0\right), \tag{12}$$

ε is the index of the space-inverse parity of the system, and $Y^{JM\varepsilon}_{jK}$ is the total symmetry-adapted angular basis function, which has the following explicit form:

$$\begin{aligned} Y^{JM\varepsilon}_{jK} = {} & \frac{1}{\sqrt{2\,(1+\delta_{K0})}} \\ & \times\left[D^{*J}_{MK}(\alpha,\beta,\gamma)Y_{j,K}(\theta,0)\right. \\ & \left. + (-1)^{\varepsilon} D^{*J}_{M-K}(\alpha,\beta,\gamma)Y_{j,-K}(\theta,0)\right]. \end{aligned} \tag{13}$$

The total angular basis function is expressed in the body-fixed frame, where D^J_{MK} is a Wigner rotation matrix to describe the overall rotation of the complex. $Y_{j,K}(\theta,0)$ is the spherical function describing the rotation of the N_2 monomer.

The bound-state calculation program is OpenMP parallelised and the PARPACK software package [43] is applied to solve the eigenvalues and eigenfunctions of the bound states. The details of the bound-state calculation method have been described in previous works [40,41]. Because of the symmetry of the N_2 molecule, the eigenfunctions of Ar–$^{14}N_2$ and Ar–$^{15}N_2$ could be labelled with indexes (ε, j) and are divided into four symmetry blocks: (+1, odd), (+1, even), (−1, odd), and (−1, even). Each block can be solved separately. In bound-state calculation, two kinds of DVR grids are used for the corresponding basis functions [44] in Hamiltonian matrix integrals: (1) the potential-optimised discrete variable representation (PODVR) [45] for the intermolecular distance R and (2) the Gauss–Legendre quadrature for the angle part. The parameters used in the bound-state calculations for Ar–N_2 are listed in Table 1.

Table 1. Parameters for Ar–N_2 are used in the bound-state calculations. The unit of R_{min} and R_{max} is bohr.

	J	j_{max}	$N_{Gauss-Legendre}$	N_{PODVR}	R_{min}	R_{max}
Ar–$^{14}N_2$	5	90	100	50	5.0	22.0
Ar–$^{15}N_2$	6	90	100	50	5.0	22.0
Ar–$^{14}N^{15}N$	5	90	100	50	5.0	22.0

3. Results and discussion

3.1 Ab initio PES

Figure 1 displays the contour plots of the intermolecular PES V_{00} for the Ar–N_2 complex. From Figure 1, one can see that there is a global minimum and two equivalent linear saddle points. The global minimum is T-shaped and has a well depth of $-98.779\ \mathrm{cm}^{-1}$ located at $R = 3.715$ Å and $\theta = 90.0°$. The two equivalent linear saddle points are located at $R = 4.260$ Å and $\theta = 0.0°$ or $\theta = 180.0°$ with a barrier height of $23.538\ \mathrm{cm}^{-1}$ relative to the global minimum. The geometries and energies of these special points for the Ar–N_2 complex are given in Table 2, including the previous results for comparison. As seen in Table 2, the global minimum on each PES is predicted to be a T-shaped structure, which is in agreement with the experiment result [4]. Compared with the empirical PESs, the potential energy of the global T-shaped minimum of the V_{00} PES recovers a depth of about 96.1% for the CPV PES [46], 88.1% for the BTT PES [47], 92.8% for the MMSV PES [48], and 96.4% for the XC3 PES [49]; the difference in the coordinate R is −0.145 Å between the CPV PES and the V_{00} PES, −0.065 Å between the

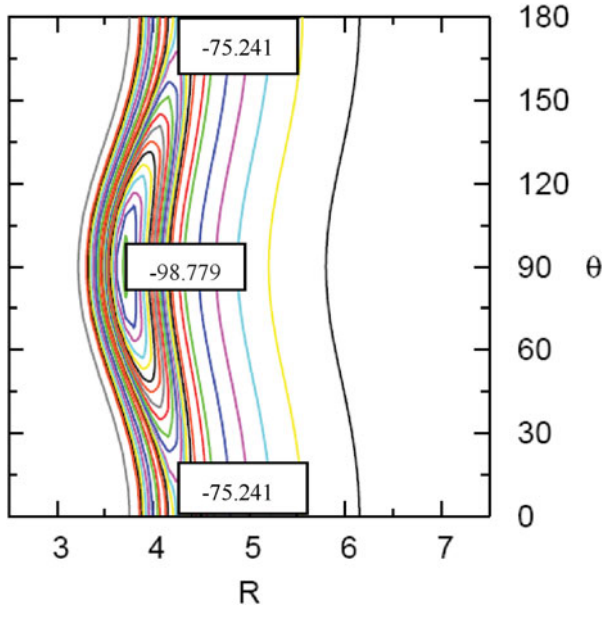

Figure 1. Contour plots of V_{00} PES for Ar–N_2, R in angstroms, θ in degrees and energy in cm^{-1}.

Table 2. Important geometries and their corresponding energies on different PESs for Ar–N_2(R in angstrom and energy in cm^{-1}).

PES		CPV[a]	BTT[b]	MMSV[c]	XC3[d]	rAPES[e]
T-shaped global minimum	R	3.570	3.650	3.680	3.726	3.696
	Energy	− 102.836	− 112.111	− 106.465	− 102.513	− 101.594
Linear Saddlepoint	R	3.960	4.310	4.280	4.370	4.242
	Energy	− 70.735	− 65.815	60.895	− 56.862	− 77.994
PES		MTE[f]	Zhu[g]	Munteanu[h]	Munteanu[i]	V_{00}
T-shaped global minimum	R	3.700	3.700	3.709	3.701	3.715
	Energy	− 104.796	− 99.997	− 99.01	− 102.5	− 98.779
Linear Saddlepoint	R	4.260	4.260	4.260	4.247	4.260
	Energy	− 80.101	− 78.478	− 75.28	− 79.73	− 75.241

From Ref. [46].
[b]From Ref. [47].
[c]From Ref. [48].
[d]From Ref. [49].
[e]From Ref. [7].
[f]From Ref. [8].
[g]From Ref. [10].
[h]PES constructed using aug-cc-pV5Z-33211 by Munteanu, from Ref. [9].
[i]PES constructed using daug-cc-pVQZ-33221 by Munteanu, from Ref. [9].

Table 3. The intermolecular vibrational energy levels and frequencies (in cm^{-1}) for the Ar–$^{14}N_2$complex with V_{00} PES.

J	Energy	Freq. rA PES[a]	Freq. This work	(ε, j)	No. in block
$J = 0$	− 77.09859	0.0	0.00000	(1, even)	1
	− 65.63208	11.57	11.46651	(1, odd)	1
	− 59.80407	17.41	17.29452	(1, even)	2
	− 50.58000	26.67	26.51859	(1, odd)	2

Note: [a]From Ref. [7].

Table 4. The average structural parameters for both $\sum^e(0)$ levels and $\Pi^e(1)$ levels of the Ar–N_2 complex (R in angstrom and angle in degree).

System	PES	$\sum^e(0)$levels $<R>$	$\sum^e(0)$levels $<\theta>$	$\Pi^e(1)$levels $<R>$	$\Pi^e(1)$levels $<\theta>$
Ar–$^{14}N_2$	CPV[a]	3.711	69.8204	3.706	70.7895
	BTT[b]	3.816	72.4824	3.813	72.8924
	MMSV[c]	3.859	71.0243	3.856	71.5842
	Expt.[d]	3.8648	68.0768	–	69.2202
	This work	3.8683	68.1265	3.859	69.5506
Ar–$^{15}N_2$	CPV[a]	3.706	70.2369	3.703	71.0865
	BTT[b]	3.811	72.8315	3.808	73.1937
	MMSV[c]	3.855	71.3623	3.852	71.8599
	Expt.[d]	3.859	–	–	–
	This work	3.864	68.5216	3.855	69.7968
Ar–$^{14}N^{15}N$	CPV[a]	3.708	70.0337	3.705	70.9375
	BTT[b]	3.813	72.6562	3.811	73.0425
	MMSV[c]	3.857	71.1927	3.853	71.7184
	Expt.[d]	–	68.2649	–	–
	This work	3.866	68.3205	3.857	69.6675

From Ref. [46].
[b]From Ref. [47].
[c]From Ref. [48].
[d]From Ref. [4].

BTT PES and the V_{00} PES, −0.035 Å between the MMSV PES and the V_{00} PES, and 0.011 Å between the XC3 PES and the V_{00} PES. Compared with the *ab initio* PESs, the potential energy of the global T-shaped minimum of the V_{00} PES recovers a depth of about 97.2% for the rA PES, 94.3% for the MTE PES, 98.8% for the PES constructed by Zhu, 99.8% for the PES constructed using aug-cc-pV5Z-33211 by Munteanu, and 96.3% for the PES constructed using daug-cc-pVQZ-33221 by Munteanu; the difference in the coordinate R is −0.019 Å between the rA PES and the V_{00} PES, −0.015 Å between the MTE PES and the V_{00} PES, −0.015 Å between the PES constructed by Zhu and the V_{00} PES, −0.006 Å between the PES constructed using aug-cc-pV5Z-33211 by Munteanu and the V_{00} PES, and −0.014 Å between the PES constructed using daug-cc-pVQZ-33221 by Munteanu and the V_{00} PES. We can see the well depth and distance at the minimum energy configuration of the V_{00} PES are very close to that of the other PESs. The main features of the V_{00} PES containing the global minimum and linear saddle points are in good agreement with other existing PESs for Ar–N_2.

3.2 Intermolecular vibrational states

The rovibrational energy levels and their corresponding wavefunctions for the Ar–N_2complex were obtained by performing bound-state calculations. The energy levels, vibrational frequencies, their corresponding indices (ε, j), and the number of roots in the block are summarised in Table 3 for the first four vibrational levels ($J = 0$) of Ar–$^{14}N_2$ with the V_{00} PES; the contour plots of the corresponding wavefunctions are shown in Figure 2. From Figure 2, we can see that intermolecular vibrational states (n) cannot be assigned as the stretching mode and bending mode (n_s, n_b), because the wavefunctions are delocalised and vibrational modes are mixed heavily.

The ground state (n=0) which is the first root in the (1, even) block is bound by energy −77.099 cm^{-1}, indicating

Table 5. Calculated pure rotational energy levels (in cm^{-1}) of the Ar–$^{14}N_2$ complex.

$J_{tot}=0$		$J_{tot}=1$		$J_{tot}=2$		$J_{tot}=3$		$J_{tot}=4$		$J_{tot}=5$	
0_{00}	−77.09859	1_{01}	−76.96292	2_{02}	−76.69163	3_{03}	−76.28481	4_{04}	−75.74261	5_{05}	−75.06522
		1_{11}	−74.52819	2_{12}	−74.26242	3_{13}	−73.86389	4_{14}	−73.33277	5_{15}	−72.66927
		1_{10}	−74.52380	2_{11}	−74.24924	3_{12}	−73.83752	4_{13}	−73.28878	5_{14}	−72.60318
				2_{21}	−67.40992	3_{22}	−67.01069	4_{23}	−66.47876	5_{24}	−65.81443
				2_{20}	−67.40990	3_{21}	−67.01057	4_{22}	−66.47838	5_{23}	−65.81353
						3_{31}	−64.86414	4_{32}	−64.35249	5_{33}	−63.71327
						3_{30}	−60.19185	4_{31}	−59.79471	5_{32}	−59.28048
								4_{41}	−59.41473	5_{42}	−58.75075
								4_{40}	−58.23083	5_{41}	−57.48470
										5_{51}	−54.83482
										5_{50}	−54.83468

that the corresponding zero point energy is 21.680 cm^{-1}. Because the zero point energy is only 1.858 cm^{-1} lower than the barrier, the wavefunctions are delocalised and quantum tunnelling occurs. The first excited vibrational state ($n=1$), which has a bound energy of −65.632 cm^{-1}, is the first root in the (1, odd) block and corresponds to the bending excitation, analysing the wavefunction. The bend vibrational frequency is 11.467 cm^{-1}. The second ($n=2$) and third ($n=3$) excited vibrational states are a combination of stretching and bending modes. From Table 3, we can also see that the three frequencies from the rA PES are 11.57 cm^{-1} (this work 11.467 cm^{-1}), 17.41 cm^{-1} (this work 17.295 cm^{-1}), and 26.67 cm^{-1} (this work 26.519 cm^{-1}), which show that our calculated frequencies agree well with those from the rA PES.

3.3 Averaged structure parameters

The average structural parameters $\langle R\rangle$ and $\langle\theta\rangle$ for a vibrational state can be determined from the related wavefunctions using the following formulae [50]:

$$\left\langle \frac{1}{R^2} \right\rangle \approx \frac{1}{\langle R^2\rangle} \text{ and } P_2\left(\cos\langle\theta\rangle\right) = \langle P_2\left(\cos\theta\right)\rangle\,, \quad (14)$$

Table 6. Calculated pure rotational energy levels (in cm^{-1}) of the Ar–$^{15}N_2$ complex.

$J_{tot}=0$		$J_{tot}=1$		$J_{tot}=2$		$J_{tot}=3$		$J_{tot}=4$		$J_{tot}=5$	
0_{00}	−77.56320	1_{01}	−77.43260	2_{02}	−77.17145	3_{03}	−76.77983	4_{04}	−76.25787	5_{05}	−75.60575
		1_{11}	−75.18718	2_{12}	−74.93134	3_{13}	−74.54769	4_{14}	−74.03639	5_{15}	−73.39762
		1_{10}	−75.18297	2_{11}	−74.91871	3_{12}	−74.52242	4_{13}	−73.99423	5_{14}	−73.33431
				2_{21}	−68.56765	3_{22}	−68.18320	4_{23}	−67.67092	5_{24}	−67.03110
				2_{20}	−68.56763	3_{21}	−68.18309	4_{22}	−67.67061	5_{23}	−67.03036
						3_{31}	−65.62713	4_{32}	−65.13372	5_{33}	−64.51727
						3_{30}	−61.36433	4_{31}	−60.96112	5_{32}	−60.44753
								4_{41}	−60.67109	5_{42}	−60.03191
								4_{40}	−59.17768	5_{41}	−58.47736
										5_{51}	−56.81288
										5_{50}	−56.81279

Table 7. Calculated pure rotational energy levels (in cm^{-1}) of the Ar–$^{14}N^{15}N$ complex.

$J_{tot}=0$		$J_{tot}=1$		$J_{tot}=2$		$J_{tot}=3$		$J_{tot}=4$		$J_{tot}=5$	
0_{00}	−77.33159	1_{01}	−77.19854	2_{02}	−76.93248	3_{03}	−76.53551	4_{04}	−76.00175	5_{05}	−75.33740
		1_{11}	−74.85888	2_{12}	−74.59823	3_{13}	−74.20738	4_{14}	−73.68648	5_{15}	−73.03573
		1_{10}	−74.85459	2_{11}	−74.58535	3_{12}	−74.18160	4_{13}	−73.64347	5_{14}	−72.97114
				2_{21}	−67.99044	3_{22}	−67.59883	4_{23}	−67.07704	5_{24}	−66.42536
				2_{20}	−67.99041	3_{21}	−67.59872	4_{22}	−67.07670	5_{23}	−66.42455
						3_{31}	−65.24746	4_{32}	−64.74530	5_{33}	−64.11793
						3_{30}	−60.77876	4_{31}	−60.37814	5_{32}	−59.86424
								4_{41}	−60.04813	5_{42}	−59.39705
								4_{40}	−58.71206	5_{41}	−57.98965
										5_{51}	−55.82653
										5_{50}	−55.82642

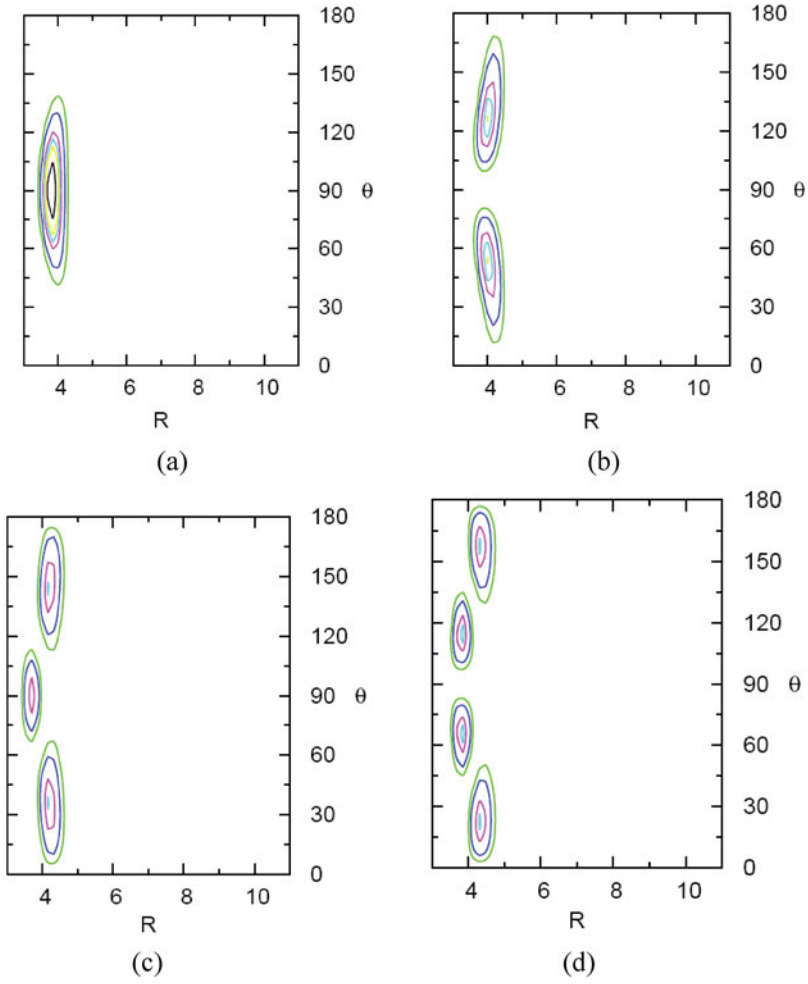

Figure 2. Contour plots of the wavefunctions for the first four vibrational levels ($J = 0$) of Ar–$^{14}N_2$ with V_{00} PES. The quantum number n is the intermolecular vibrational state. R in angstroms and θ in degrees. (a) $n = 0$; (b) $n = 1$; (c) $n = 2$; (d) $n = 3$.

where P_2 is the second-order Legendre function and $\langle P_2(\cos\theta)\rangle$ is the averaged value of the Legendre function for the state of interest. The calculated structural parameters of the Ar–N_2 complex for both $\sum^e(0)$ and $\Pi^e(1)$levels are listed in Table 4.

For $\sum^e(0)$ levels of Ar–$^{14}N_2$, the averaged structural parameters $\langle R\rangle$ and $\langle\theta\rangle$ of empirical PESs deviate from the experimental results: −0.1538 Å/1.7436° for the CPV PES, −0.0488 Å/4.4056° for the BTT PES, and −0.0058 Å/2.9475° for the MMSV PES; with our calculations the errors are reduced to 0.0035 Å/0.0497°. For $\Pi^e(1)$ levels, the difference of the average value of the angle θ between our calculation and experimental results is 0.3304° which is smaller than that between empirical PESs and experimental results. For Ar–$^{15}N_2$ and Ar–$^{14}N^{15}N$, our calculations agree well with experimental results and those obtained with empirical PESs.

It is very interesting to compare the structural parameters between the minimum on PES and the vibrational averaged values of the ground state. For $\sum^e(0)$ levels, the intermolecular distances deviate slightly from the minimum on PES, 0.1533 Å for Ar–$^{14}N_2$, 0.149 Å for Ar–$^{15}N_2$, and 0.151 Å for Ar–$^{14}N^{15}N$, reflecting the effects of small-amplitude motion and zero point energy. The value of $\langle\theta\rangle$ reflects the average bending vibration in the Ar–N_2 complex. The large deviations of $\langle\theta\rangle$ from their equilibrium values can be considered the effect of the hindered rotation of the N_2 monomer in the complex, because the interaction between the Ar atom and the N_2 molecule is so weak that the N_2 monomer cannot be bounded at its equilibrium geometry.

3.4 Rotational analysis

In this work, we use (v, n) to describe the vibrational state of the Ar–N_2 complex, where v is the intramolecular vibrational state corresponding to the N_2 monomer

Table 8. Calculated microwave transition frequencies (in MHz)from 3d-aVQZ compared to experiment data and *ab initio* data from 2d-aVQZ for Ar–$^{14}N_2$ and ^{84}Kr–$^{14}N_2$ complexes.

$J'_{k'_a k'_c} - J''_{k''_a k''_c}$	Expt.[a]	2d-aVQZ[b]	Calc.(2d)-expt.	3d-aVQZ[c]	Calc.(3d)-expt.
Ar–$^{14}N_2$					
$1_{01}-0_{00}$	4105.499	4064.9	− 40.599	4067.278	− 38.221
$2_{02}-1_{01}$	8209.580	8128.5	− 81.080	8133.057	− 76.523
$3_{03}-2_{02}$	12310.814	12189.1	− 121.714	12196.138	− 114.676
$4_{04}-3_{03}$	16407.774	16245.5	− 162.274	16254.722	− 153.052
$5_{05}-4_{04}$	–	20296.2	–	20307.610	–
$2_{12}-1_{11}$	8042.008	7963.4	− 78.608	7967.571	− 74.437
$3_{13}-2_{12}$	12059.103	11941.1	− 118.003	11947.610	− 111.493
$4_{14}-3_{13}$	16071.494	15914.1	− 157.394	15922.552	− 148.942
$5_{15}-4_{14}$	–	19880.8	–	19891.199	–
$2_{11}-1_{10}$	8308.429	8226.3	− 82.129	8231.089	− 77.340
$3_{12}-2_{11}$	12459.242	12336.0	− 123.242	12343.036	− 116.206
$4_{13}-3_{12}$	16605.969	16441.7	− 164.269	16450.786	− 155.184
$5_{14}-4_{13}$	–	20541.8	–	20553.740	–
RMSE	–	119.651	–	112.967	–
^{84}Kr–$^{14}N_2$					
$J'_{k'_a k'_c} - J'_{k'_a k'_c}$	Expt.[d]	2d-aVQZ[e]	Calc.(2d)-expt.	3d-aVQZ[f]	Calc.(3d)-expt.
$2_{02}-1_{01}$	6035.269	5972.166	− 63.103	5975.463	− 59.806
$3_{03}-2_{02}$	9051.322	8956.599	− 94.723	8961.696	− 89.626
$4_{04}-3_{03}$	12065.473	11939.235	− 126.238	11945.830	− 119.643
$5_{05}-4_{04}$	15077.082	14917.973	− 159.109	14927.566	− 149.516
$2_{12}-1_{11}$	5951.889	5890.322	− 61.567	5893.620	− 58.269
$3_{13}-2_{12}$	8926.129	8833.984	− 92.145	8838.781	− 87.348
$4_{14}-3_{13}$	11898.319	11775.548	− 122.771	11781.844	− 116.475
$5_{15}-4_{14}$	14867.764	14712.914	− 154.850	14722.508	− 145.256
$2_{11}-1_{10}$	6091.215	6027.028	− 64.187	6030.625	− 60.590
$3_{12}-2_{11}$	9135.304	9039.342	− 95.962	9044.439	− 90.865
$4_{13}-3_{12}$	12177.568	12049.558	− 128.010	12056.154	− 121.414
$5_{14}-4_{13}$	15217.394	15056.177	− 161.217	15065.770	− 151.624
RMSE	–	115.918	–	109.403	–

[a]From Ref. [4].
[b]From Ref. [9].
[c]This work.
[d]From Ref. [13].
[e]From Ref. [18].
[f]From Ref. [19].

and n is the intermolecular vibrational state of the Ar–N_2 complex. The rotational energy levels of the vibrational state (v, n) = (0, 0) with J = 0–5 for Ar–$^{14}N_2$, Ar–$^{15}N_2$, and Ar–$^{14}N^{15}N$ complexes are calculated and their assignments are listed in Tables 5–7. The theoretical transition frequencies of these complexes are listed in Tables 8 and 9. In Tables 8 and 9, 2d-aVQZ represents a two-dimensional PES constructed using CCSD(T) and the aug-cc-pVQZ basis set with a set of 3*s*3*p*2*d*2*f*1*g* mid-bond functions, 3d-aVQZ represents a three-dimensional PES constructed using the same method and basis set as used in our work; Wang's two-dimensional PES [18] and Zhang's three-dimensional PES [19] of the ^{84}Kr–$^{14}N_2$ complex were constructed using the CCSD(T) method, the basis sets being aug-cc-pVQZ-PP for the Kr atom and aug-cc-pVQZ for the N atom. It can be seen that the *ab initio* calculated results of 2d-aVQZ and 3d-aVQZ are smaller than the experiment results and all the RMSEs of 3d-aVQZ PESs are smaller than those of 2d-aVQZ PESs with a value of 7 MHz, reflecting that the vibrationally averaged PESs of Ar–N_2 and ^{84}Kr–$^{14}N_2$ give more accurate results.

In order to compare the spectroscopic parameters with experimental values directly, the theoretical transition frequencies are fitted with the same Hamiltonian as used in the experiment, a Watson asymmetric rotor expression employing the S-type reduction in the *I*–*r* representation [51],

$$H = \frac{1}{2}(B+C)J^2 + \left[A - \frac{1}{2}(B+C)\right]J_a^2 + \frac{1}{2}(B-C)\left(J_b^2 - J_c^2\right) - \Delta_J J^4 - \Delta_{JK} J_a^2 J^2 - \Delta_K J_a^4 + \delta_J J^2\left(J_+^2 - J_-^2\right) + \delta_K\left(J_+^4 - J_-^4\right) + H_J J^6 + H_{JK} J^4 J_a^2 + H_{KJ} J^2 J_a^4 + H_K J_a^6. \quad (15)$$

The determined parameters for Ar–$^{14}N_2$ and Ar–$^{15}N_2$ are listed in Table 10, which show a good agreement with

Table 9. Calculated microwave transition frequencies(in MHz) from 3d-aVQZ compared to experiment data and *ab initio* data from 2d-aVQZ for Ar–$^{15}N_2$ and Ar–$^{14}N^{15}N$ complexes.

$J'_{k'_a k'_c} - J'_{k'_a k'_c}$	Expt.[a]	2d-aVQZ[b]	Calc.(2d)-expt.	3d-aVQZ[c]	Calc.(3d)-expt.
Ar–$^{15}N_2$					
$1_{01}-0_{00}$	3952.023	3913.1	−38.923	3915.284	−36.739
$2_{02}-1_{01}$	7902.740	7824.9	−77.840	7829.068	−73.672
$3_{03}-2_{02}$	11850.842	11734.1	−116.742	11740.454	−110.388
$4_{04}-3_{03}$	15795.013	15639.4	−155.613	15647.943	−147.070
$5_{05}-4_{04}$	19733.926	19539.4	−194.526	19550.035	−183.891
$6_{06}-5_{05}$	–	23432.9	–	23445.533	–
$2_{12}-1_{11}$	7741.000	7666.1	−74.900	7669.879	−71.121
$3_{13}-2_{12}$	11608.660	11495.5	−113.160	11501.520	−107.140
$4_{14}-3_{13}$	15471.597	15320.7	−150.897	15328.365	−143.232
$5_{15}-4_{14}$	19328.820	19140.2	−188.620	19149.814	−179.006
$6_{16}-5_{15}$	–	22952.4	–	22964.067	–
$2_{11}-1_{10}$	7996.943	7918.0	−78.943	7922.303	−74.640
$3_{12}-2_{11}$	11992.291	11873.9	−118.391	11880.457	−111.834
$4_{13}-3_{12}$	15983.871	15826.0	−157.871	15834.714	−149.157
$5_{14}-4_{13}$	19970.417	19773.0	−197.417	19783.874	−186.544
$6_{15}-5_{14}$	–	23713.7	–	23726.738	–
RMSE	–	137.048	–	129.683	–
Ar–$^{14}N^{15}N$					
$1_{01}-0_{00}$	4026.305	3986.5	−39.805	3988.733	−37.572
$2_{02}-1_{01}$	8051.248	7971.6	−79.648	7976.266	−74.982
$3_{03}-2_{02}$	12073.464	11953.9	−119.564	11960.801	−112.663
$4_{04}-3_{03}$	16091.581	15932.2	−159.381	15941.739	−149.842
$5_{05}-4_{04}$	–	19905.0	–	19916.682	–
RMSE	–	109.117	–	102.688	–

[a]From Ref. [4].
[b]From Ref. [9].
[c]This work.

the corresponding experimental values. In Table 10, the inertial defects are also listed. We can see that the calculated values of the inertial defects are a little larger than the corresponding experimental values, with a discrepancy of 0.104 amu Å^2 for the Ar–$^{14}N_2$ complex and 0.109 amu Å^2 for the Ar–$^{15}N_2$ complex.

4. Conclusions

Ab initio calculation for the Ar–N_2 complex is performed using CCSD(T) and the aug-cc-pVQZ basis set for all atoms with midbond functions (3*s*3*p*2*d*2*f*1*g*). Compared with previous PESs [5–11], the N_2 bond length is varied over five values; the first three-dimensional PES is constructed using the NN fitting method. By performing a potential integral, a vibrationally averaged two-dimensional PES is obtained. The vibrationally averaged PES V_{00} could be characterised by a global T-shaped minimum, two equivalent local linear saddle points.

Bound states are performed for the Ar–$^{14}N_2$, Ar–$^{15}N_2$, and Ar–$^{14}N^{15}N$ van der Waals complexes; intermolecular vibrational states for Ar–$^{14}N_2$ are assigned from the analysis of their wavefunctions. The calculated values of average structural parameters are in agreement with experimental results and the pure rotational energy levels up to $J = 5$ are obtained. The theoretical rotational transition frequencies are compared with experimental values

Table 10. Comparison of spectroscopic parameters for Ar–N_2.

	Ar–$^{14}N_2$		Ar–$^{15}N_2$	
Parameter	Expt.[a]	This work	Expt.[a]	This work
A (MHz)	69130.0	69130.0	64550.0	64550.0
B (MHz)	2119.3889(6)	2099.4912	2039.9157(17)	2020.7334
C (MHz)	1986.3155(6)	1968.0313	1912.2881(17)	1894.6490
Δ_J (KHz)	50.956 (13)	53.428	46.07 (7)	45.14
Δ_{JK} (KHz)	8576.1 (4)	8439.103	8373.2 (10)	8228.4
δ_J (KHz)	−4.262 (10)	−5.131	−3.460 (16)	−3.684
H_J (KHz)	–	–	−0.0054 (14)	−0.0228
H_{JK} (KHz)	−7.938 (16)	−7.748	−7.327 (26)	−7.898
Inertial defect (amu Å^2)	8.665	8.769	8.705	8.814

Note: [a]From Ref. [4].

and previous results of other groups. The RMSEs between calculated and experimental results confirm the higher accuracy of our *ab initio* three-dimensional PES.

Acknowledgements

The authors thank Prof. Minghui Yang for providing the computer used to perform the calculations in this study.

Disclosure statement

No potential conflict of interest was reported by the authors.

Funding

This work was supported by the Science Foundation for Introducing Talent of Ningde Normal University (Grant No. 2013Y004); the Education and Research Foundation (Science and Technology) for Young Teachers of the Education Department of Fujian Province [Grant No. JA15557]; the Scientific Innovation Team Foundation of Ningde Normal University [Grant No. 2013T03]; the National Science Foundation of China [Grant No. 21303254]; the National Natural Science Foundation of China [Grant No. 11304095].

References

[1] G. Henderson and G.E. Ewing, Mol. Phys. **27**, 903 (1974).
[2] A.R.W. McKellar, J. Chem. Phys. **88**, 4190 (1988).
[3] W. Jäger, and M.C.L. Gerry, Chem. Phys. Lett. **196**, 274 (1992).
[4] W. Jäger, M.C.L. Gerry, C. Bissonnette, and F.R.W. McCourt, Faraday Discuss. **97**, 105 (1994).
[5] Z. Slanina, S.J. Kim, and K. Fox, J. Mol. Struct.: Theochem. **288**, 17 (1993).
[6] F.Y. Naumkin, Mol. Phys. **90**, 875 (1997).
[7] B. Fernández, H. Koch, and J. Makarewicz, J. Chem. Phys. **110**, 8525 (1999).
[8] K. Patel, P.R. Butler, A.M. Ellis, and M.D. Wheeler, J. Chem. Phys. **119**, 909 (2003).
[9] C.R. Munteanu, J.L. Cacheiro, and B. Fernández, J. Chem. Phys. **121**, 10419 (2004).
[10] J. Zhu, Y.-P. Lu, X.-R. Chen, and Y. Cheng, Eur. Phys. J. D **33**, 43 (2005).
[11] A.K. Dham, W.J. Meath, J.W. Jechow, and F.R.W. McCourt, J. Chem. Phys. **124**, 034308 (2006).
[12] W. Jäger, Y. Xu, G. Armstrong, M.C.L. Gerry, F.Y. Naumkin, F. Wang, and F.R.W. McCourt, J. Chem. Phys. **109**, 5420 (1998).
[13] W. Jäger, Y. Xu, N. Heineking, and M.C.L. Gerry, J. Chem. Phys. **99**, 7510 (1993).
[14] Q. Wen and W. Jäger, J. Chem. Phys. **122**, 214310 (2005).
[15] A.K. Dham and W.J. Meath, Mol. Phys. **99**, 991 (2001).
[16] C.R. Munteanu, J.L. Cacheiro, and B. Fernández, J. Chem. Phys. **120**, 9104 (2004).
[17] A.K. Dham and W.J. Meath, Chem. Phys. **196**, 125 (1995).
[18] Z. Wang, M. Niu, E. Feng, H. Yu, J. Du, and J. Ma, Chem. Phys. Lett. **484**, 124 (2010).
[19] C. Zhang, Z. Wang, and E. Feng, Chem. Phys. Lett. **517**, 16 (2011).
[20] J. Bechler, Phys. Chem. Chem. Phys. **13**, 17930 (2011).
[21] C. Hampel, K. Peterson, and H.J. Werner, Chem. Phys. Lett. **190**, 1 (1992).
[22] R.R. Toczylowski and S.M. Cybulski, J. Chem. Phys. **112**, 4604 (2000).
[23] S.F. Boys and F. Bernardi, Mol. Phys. **19**, 553 (1970).
[24] H.-J. Werner, P.J. Knowles, G. Knizia, F.R. Manby, M. Schütz, P. Celani, T. Korona, R. Lindh, A. Mitrushenkov, G. Rauhut, K.R. Shamasundar, T.B. Adler, R.D. Amos, A. Bernhardsson, A. Berning, D.L. Cooper, M.J.O. Deegan, A.J. Dobbyn, F. Eckert, E. Goll, C. Hampel, A. Hesselmann, G. Hetzer, T. Hrenar, G. Jansen, C. Köppl, Y. Liu, A.W. Lloyd, R.A. Mata, A.J. May, S.J. McNicholas, W. Meyer, M.E. Mura, A. Nicklaß, D.P. O'Neill, P. Palmieri, D. Peng, K. Pflüger, R. Pitzer, M. Reiher, T. Shiozaki, H. Stoll, A.J. Stone, R. Tarroni, T. Thorsteinsson, and M. Wang, *MOLPRO, Version 2010. 1: A Package of Ab Initio Programs* (2010). <http://www.molpro.net>.
[25] B. Jiang and H. Guo, J. Chem. Phys. **139**, 054112 (2013).
[26] J. Li, B. Jiang, and H. Guo, J. Chem. Phys. **139**, 204103 (2013).
[27] J. Li, J. Chen, D.H. Zhang, and H. Guo, J. Chem. Phys. **140**, 044327 (2014).
[28] J. Chen, X. Xu, X. Xu, and D.H. Zhang, J. Chem. Phys. **138**, 154301 (2013).
[29] J. Chen, X. Xu, X. Xu, and D.H. Zhang, J. Chem. Phys. **138**, 221104 (2013).
[30] X. Xu, J. Chen, and D.H. Zhang, Chin. J. Chem. Phys. **27**, 373 (2014).
[31] W. Koch and D.H. Zhang, J. Chem. Phys. **141**, 021101 (2014).
[32] M.T. Hagan and M.B. Menhaj, IEEE Trans. Neural New. **5**, 989 (1994).
[33] W.S. Sarle, *Proceedings of the 27th Symposium on the Interface of Computing Science and Statistics* (Interface Foundation of North America, Pittsburgh, PA, 2005), p. 352.
[34] T.B. Pedersen, J.L. Cacheiro, B. Fernández, and H. Koch, J. Chem. Phys. **117**, 6562 (2002).
[35] K.A. Peterson and G.C. McBane, J. Chem. Phys. **123**, 084314 (2005).
[36] Z. Wang, M. Gong, Y. Zhang, E. Feng, and Z. Cui, Chem. Phys. Lett. **454**, 7 (2008).
[37] E. Feng, Y. Zhang, Z. Wang, M. Niu, and Z. Cui, J. Chem. Phys. **13**, 124311 (2009).
[38] Z. Wang, E. Feng, H. Yu, C. Zhang, and J. Du, J. Chem. Phys. **134**, 024320 (2011).
[39] B.K. Taylor and R.J. Hinde, J. Chem. Phys. **122**, 074308 (2005).
[40] L.M. Zang, W. Dai, L.M. Zheng, C.X. Duan, Y.P. Lu, and M.H. Yang, J. Chem. Phys. **140**, 114310 (2014).
[41] H. Fu, J. Lv, L.M. Zheng, and R. Zheng, J. Mol. Spectrosc. **311**, 100 (2015).
[42] J. Bendtsen, J. Raman Spectrosc. **2**, 133 (1974).
[43] R. Lehoucq, D.C. Sorensen, and C. Yang, *ARPACK User's Guide: Solution of Large-Scale Eigenvalue Problems with Implicitly Restarted Arnoldi Methods* (SIAM, Philadelphia, PA, 1998). <http://www.caam.rice.edu/software/ARPACK>.
[44] R.B. Lehoucq, S.K. Gray, D.H. Zhang, and J.C. Light, Comput. Phys. Commum. **109**, 15 (1998).
[45] J. Echave and D.C. Clary, Chem. Phys. Lett. **190**, 225 (1992).

[46] R. Candori, F. Priani, and F. Vecchiocattivi, Chem. Phys. Lett. **102**, 412 (1983).
[47] M.S. Bowers, K.T. Tang, and J. Peter Toennies, J. Chem. Phys. **88**, 5465 (1988).
[48] L. Beneventi, P. Casavecchia, G.G. Volpi, C.C.K. Wong, and F.R.W. McCourt, J. Chem. Phys. **98**, 7926 (1993).
[49] A.K. Dham, F.R.W. McCourt, and W.J. Meath, J. Chem. Phys. **103**, 8477 (1995).
[50] H. Ran, Y.Z. Zhou, and D.Q. Xie, J. Chem. Phys. **126**, 204304 (2007).
[51] M.J. Weida, J.M. Sperhac, D.J. Nesbitt, and J.M. Hutson, J. Chem. Phys. **101**, 8351 (1994).